Preprint submitted to Nuclear Instruments and Methods A

Germanium-gated γ–γ fast timing of excited states in fission fragments using the EXILL&FATIMA spectrometer

J.-M. Régis [a,*], G.S. Simpson [b,c,**], A. Blanc [d], G. de France [e], M. Jentschel [d], U. Köster [d], P. Mutti [d], V. Paziy [f], N. Saed-Samii [a], T. Soldner [d], C.A. Ur [g], W. Urban [d,h], A.M. Bruce [i], F. Drouet [b], L.M. Fraile [f], S. Ilieva [j], J. Jolie [a], W. Korten [k], T. Kröll [j], S. Lalkovski [l], H. Mach [f,m], N. Mărginean [n], G. Pascovici [a], Zs. Podolyak [o], P.H. Regan [o], O.J. Roberts [i], J.F. Smith [c], C. Townsley [o], A. Vancraeyenest [b], N. Warr [a]

[a] Institut für Kernphysik der Universität zu Köln, Zülpicher Str. 77, 50937 Köln, Germany
[b] Laboratoire de Physique Subatomique et de Cosmologie Grenoble, 53, rue des Martyrs, 38026 Grenoble Cedex, France
[c] School of Engineering, University of the West of Scotland, Paisley PA1 2BE, Scotland
[d] Institut Laue-Langevin, CS 20156, 38042 Grenoble Cedex 9, France
[e] Grand Accélérateur National d'Ions Lourds, Bd Henri Becquerel, BP 55027, 14076 Caen Cedex 05, France
[f] Grupo de Física Nuclear, FAMN, Universidad Complutense, CEI Moncloa, 28040 Madrid, Spain
[g] Istituto Nazionale di Fisica Nucleare, Sezione di Padova, Via Marzolo 8, 35131 Padova, Italy
[h] Faculty of Physics, University of Warsaw, ul. Hoża 69, PL-00-681 Warsaw, Poland
[i] School of Computing, Engineering and Mathematics, University of Brighton, Brighton BN2 4GJ, United Kingdom [j] Institut für Kernphysik, Technische Universität zu Darmstadt, Schlossgartenstr. 2, 64289Darmstadt, Germany
[k] Commissariat à l'énergie atomique et aux énergies alternatives de Saclay, Route Nationale, 91400 Gif-sur-Yvette, France
[l] Faculty of Physics, University of Sofia "St. Kliment Ohridski", 1164 Sofia, Bulgaria
[m] National Centre for Nuclear Research, Division BP1, ul. Hoża 69, 00-681 Warsaw, Poland
[n] Horia Hulubei National Institute for Physics and Nuclear Engineering, 77125 Bucharest, Romania
[o] Department of Physics, University of Surrey, Guildford GU2 7XH, United Kingdom

A B S T R A C T

A high-granularity mixed spectrometer consisting of high-resolution Ge and very fast $LaBr_3(Ce)$-scintillator detectors has been installed around a fission target at the cold-neutron guide PF1B of the high-flux reactor of the Institut Laue–Langevin. Lifetimes of excited states in the range of 10 ps to 10 ns can be measured in around 100 exotic neutron-rich fission fragments using Ge-gated $LaBr_3(Ce)$–$LaBr_3(Ce)$ or Ge–Ge–$LaBr_3(Ce)$–$LaBr_3(Ce)$ coincidences. We report on various characteristics of the EXILL&FATIMA spectrometer for the energy range of 40 keV up to 6.8 MeV and present results of ps-lifetime test measurements in a fission fragment. The results are discussed with respect to possible systematic errors induced by background contributions.

Keywords:
Fast-timing arrays
$LaBr_3(Ce)$ scintillators
Lifetime measurements
The GCD method
Neutron capture gamma rays
Neutron induced fission

1. Introduction

Low-energy fission of trans-actinide nuclei produces neutron-rich, secondary fragments in the mass $80 < A < 160$ region, often in conditions suitable for spectroscopic studies using large arrays of Ge detectors [1]. This reaction gives access to a wide range of nuclei difficult to study using conventional stable-beam accelerators and fusion reactions. The nuclei of this region exhibit a number of interesting nuclear-structure phenomena. For example, low-lying states of the several $Z \sim 40$ isotopic chains in the neutron-rich $A \sim 100$ region change shape from a spherical one at neutron number $N=58$ to a strongly prolate-deformed one at $N=60$ [2]. Evidence of shape coexistence in the nuclei here has also been presented [3,4], offering the opportunity to investigate the roles played by different orbits in the onset of quadrupole deformation. This region lies close to the light peak of the double-humped fission distribution.

The nuclei ^{78}Ni and ^{132}Sn are doubly magic in the spin–orbit coupling scheme. Fission can populate isotopes just a few nucleons

* Corresponding author. Tel.: +49 221 470 3622; fax: +49 221 470 5168.

away from ^{78}Ni reasonably well. The immediate region around ^{132}Sn lies almost at the heavy-wing peak of the fission distribution. Level schemes and lifetimes obtained from spectroscopic studies in these two regions can be compared to the predictions of shell-model calculations. The evolution of nucleon–nucleon interactions and the monopole migration of effective single-particle energies in neutron-rich regions are currently subjects of much interest in nuclear-structure studies. Measurements of the lifetimes of excited states can allow precise tests of shell-model predictions, probing the different orbit occupancies of states connected by a transition. In deformed regions lifetime information explores the degree of collective behaviour present in a particular state.

Previously, lifetimes of excited-states in fission fragments have been measured using several methods. These include direct-timing methods, following β decay [5,6], though this is generally limited to studies of low-spin states. The fission reaction populates intermediate-spin states and lifetimes of these levels, and the ones below, have been determined using direct-timing methods with Ge detectors [7]. The poor timing performance of Ge detectors generally limits measurements of this type to lifetimes upwards of a ns. The characteristic Doppler broadening of γ rays emitted by fission fragments slowing down in a thick backing has been used to obtain lifetimes of intermediate-spin states in the ps range [8]. Differential plungers have also been used with spontaneous-fission sources, to obtain lifetimes in the ps-to-ns regime [9,10]. Measurements must be performed at some 10–20 plunger-source distances, effectively dividing the statistics up into the same number of data sets. The γ rays emitted from fission fragments in plunger experiments have three different energies, dependent upon the velocity of the fragment at the time they were emitted (fully shifted, partially shifted and stopped). The two γ-ray peaks emanating from in-flight decay are also Doppler broadened. Together all these effects result in complex spectra, limiting the technique for studies of fission fragments close to the peak of the fission–fragment mass distribution.

In the present article a description of the first prompt-fission γ-ray spectroscopy experiment, performed using a mixed array of Ge and Ce-doped $LaBr_3$ detectors, is presented. These detectors were placed around thin ^{235}U and ^{241}Pu targets, with thick backings, meaning that the fragments stopped in ∼1 ps. Fission was induced by cold-neutrons from the collimated neutron guide PF1B [11,12] of the reactor of the Institut Laue–Langevin (ILL). Prompt γ-ray cascades from the nuclei of interest are selected via Ge–$LaBr_3$–$LaBr_3$ or Ge–Ge–$LaBr_3$–$LaBr_3$ coincidences. Here the good energy resolution of the Ge detectors allow a precise gate, or gates, to be set, selecting the cascade of interest. Such coincidence conditions are necessary as over 100 nuclei are strongly produced in fission, each emitting ∼4 γ rays. The excellent timing performance of the $LaBr_3$ detectors allows the time difference between γ rays feeding and decaying from a state to be measured directly in the ps-to-ns range. Compared to plunger experiments, which are also able to measure lifetimes in the ps-to-ns lifetime range, the simpler spectra of the stopped fragments in this fast-timing experiment allows the half-lives of weaker transitions to be obtained. In comparison to previous experiments using ^{248}Cm, ^{252}Cf spontaneous-fission sources, the neutron-rich $A\sim80$ and ^{132}Sn regions are both better populated by the cold-neutron induced fission of ^{235}U and ^{241}Pu.

2. Set-up and performance of the EXILL&FATIMA spectrometer

2.1. Set-up

The basis of the experimental set-up is part of the EXOGAM array [13]. The central ring of the EXILL (acronym for EXOGAM at ILL) array around the target orthogonal to the beam direction has been equipped with 8 BGO-shielded EXOGAM clover detectors

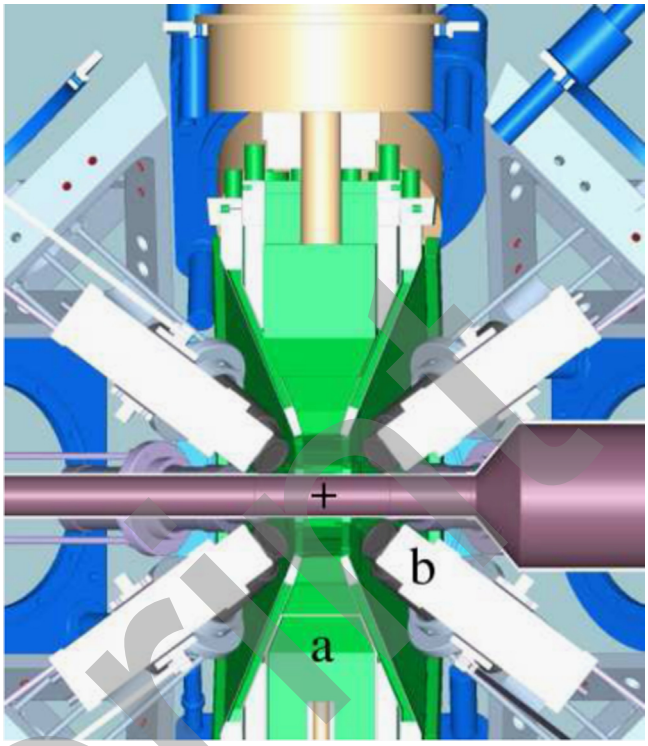

Fig. 1. CAD design of the EXILL&FATIMA spectrometer equipped with (a) BGO Compton-suppressed EXOGAM Ge-clover detectors and (b) $LaBr_3$(Ce)-scintillator detectors. Note the 3-dimensional central symmetry of the $LaBr_3$(Ce)-detector array with respect to the target position indicated with a +. The PF1B cold-neutron guide provides a halo-free neutron beam 12 mm in diameter with a high neutron flux of about $10^8/(s\times cm^2)$ at the target position [12].

(composite detectors, each made of 4 Ge crystals) with a target-to-detector distance of 14.5 cm. As illustrated in Fig. 1, two rings consisting of eight 5% Ce-doped $LaBr_3$ detectors each were installed on both sides of the central ring with detector angles of 40° and 140° relative to the beam direction. In order to provide the highest possible γ–γ ($LaBr_3$–$LaBr_3$) coincidence efficiency, the faces of the cylindrical $LaBr_3$ crystals with diameter of 1.5 in. were placed at 8.5 cm relative to the target position and were almost touching each other. The $LaBr_3$ crystals differ only slightly in their length; 8 crystals have a length of 1.5 in. while the other 8 crystals are 2 in. long. All $LaBr_3$ detectors utilise the Hamamatsu R9779 photomultiplier tube (PMT) which has superior energy and timing performance compared to previously used PMTs [14].

In order to provide the best fast-timing-array (FATIMA) time resolving power an analogue electronic "fast-timing" circuit as described in Ref. [15] was installed, consisting of constant fraction discriminators (CFD) of a single type (Ortec 935), multi channel logic fan-in/fan-out modules (FAN) and time-to-amplitude converters (TAC). This electronic set-up ensures that the TAC number $i\in[1,(N-1)]$ of the N detector timing system can only be started by detector number i and stopped by a detector number $j\in[i+1,N]$. Each time peak $TAC_{(i,j)}$ of the $N(N-1)/2$ detector combinations (i,j) with $i<j$ was individually adjusted approximately in the middle of the 50 ns-range TAC spectrum, by adjusting the cable length between the connections of the CFDs, FANs and TACs. This is made in order to allow the measurement of lifetimes up to 10 ns independent of the detectors hit and also to provide the best $LaBr_3$–$LaBr_3$ coincidence resolving time. Synchronised CAEN V1724 100 MHz digitizers were used to process and collect the energy signals of the $LaBr_3$, Ge and BGO detectors and the height of the TAC signals. Each signal is converted into an event which is stored trigger-less in a triple list-mode including

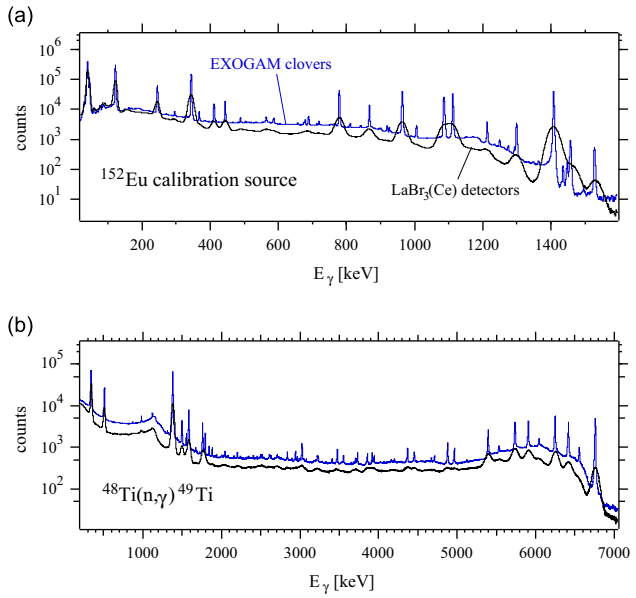

Fig. 2. Semi-logarithmic plots of superimposed calibrated spectra representing the EXILL-Ge and FATIMA-LaBr$_3$(Ce) singles γ-ray energy spectra of calibration measurements using (a) a ^{152}Eu γ-ray source and (b) the in-beam reaction ^{48}Ti(n$_{th}$,γ)^{49}Ti.

the ID of the channel, its amplitude and the time of registration (10 ns timestamp) using the digital pulse-shape algorithm described in Ref. [16]. To make this possible, the very fast LaBr$_3$ energy signals (PMT dynode output pulse with decay time of 15 ns) had to be shaped using RC-filters to provide a signal with a decay time of about 2 μs. Coincidences are established in the off-line analysis.

To investigate the long term stability and geometrical timing effects, several calibration measurements have been performed over 5 weeks with the usage of the EXILL&FATIMA spectrometer. Fig. 2 shows the comparisons of calibrated and superimposed Ge and LaBr$_3$ singles energy spectra of a standard ^{152}Eu point-like γ-ray source and the ^{48}Ti(n$_{th}$,γ)^{49}Ti reaction on a 84-mg Ti sheet with an area of about 40 mm^2. These two γ-ray emitters were used to measure various EXILL&FATIMA features for the energy range from 40 keV to 6.8 MeV, as presented in the following sections.

2.2. Data analysis using SOCOv2

A new C++ software package "SOCOv2" [17] has been developed at the Institute of Nuclear Physics of Cologne in order to standardise and simplify the analysis of trigger-less list-mode data by using a command scheme. One of the software's goals is to implement new "commands" when the need arises in order to adapt new methods and features. The SOCOv2 software is designed to fully utilise the potential computing power of multi-core processor systems by extensive parallel processing. SOCOv2 is also designed to be adaptable to the different output formats of the different digital data acquisition systems used worldwide. Channel IDs, time-correlation (peaks of timestamp-difference spectra) and multiplicity information are extracted from the raw data to create a configuration file which includes timestamp offsets for providing the best multi-coincidence resolving time. Singles spectra are built to provide polynomial calibration parameters. Gain drifts are compensated by generating linear or quadratic shift parameters using the shift-tracker tool. The trigger-less data stream is pre-sorted into events, according to the desired coincidence requirements. This event building reduces the original data size by at least one order of magnitude in order to accelerate further more specific analyses. Energy gates, either single channel or general detector type gates, are specified in a file to create multi-gated coincidence spectra. Optionally, active BGO Compton suppression and add-back reconstruction can be applied to the Ge data. The "ft-matrix" command of SOCOv2 creates two "start" and "stop" (E_γ, t) fast-timing matrices using a type gate "LaBr" as the reference energy gate. Under the assumption a TAC number i can only be started by the LaBr$_3$ number i and stopped by an LaBr$_3$ number j with $j > i$, the command can distinguish whether the reference energy gate belongs to the start or stop branch and increments the right matrix accordingly. The generated FATIMA matrices then include the superimposed information as obtained from the complete fast-timing array for performing the generalised centroid difference (GCD) method [15] (more details are given in Section 2.6). For the analysis presented hereafter, no background subtraction of any kind has been applied to the data.

2.3. Energy performance of FATIMA

As a matter of course, each individual detector has a characteristic gain. Scintillator detectors show small differences in their response voltage related to the non-proportional scintillation light yield of the crystal and gain variances of the PMT [18]. In order to be able to perform fast timing using γ-ray energies down to 40 keV, the amplitudes of the PMT-anode outputs were adjusted to −1 V per MeV γ-ray energy corresponding to a PMT supply voltage of about −1400 V. Fig. 3 presents the two extreme LaBr$_3$-detector energy responses of the FATIMA set-up, as obtained using data from the ^{48}Ti(n$_{th}$,γ)^{49}Ti reaction. Up to 3 MeV corresponding to a PMT-anode amplitude of −3 V, the FATIMA-LaBr$_3$ detectors have about the same, nearly linear, energy response. Above 3 MeV, the energy response becomes non-linear dependent on the detector. The non-linearity above 3 MeV is however relatively weak. The relative FATIMA energy resolution as a function of the energy, presented in Fig. 4, was obtained from the full width at half maximum (FWHM) of full-energy peaks in the spectrum of the superposition of the 16 calibrated LaBr$_3$ spectra as shown in Fig. 2. The solid curve shown in Fig. 4 represents the ideal relative energy resolution as obtained for a linear energy response [18]. At the ^{137}Cs energy of 662 keV, the relative energy resolution of the FATIMA set-up is 3.3%.

2.4. Full-energy peak efficiencies

A ^{152}Eu point-like γ-ray source with activity of 362 kBq was used to measure absolute efficiencies in the energy region of 122–1408 keV. For the high energy region (787–6.1 MeV), the reaction ^{35}Cl(n$_{th}$,γ)^{36}Cl was used and relative efficiencies were

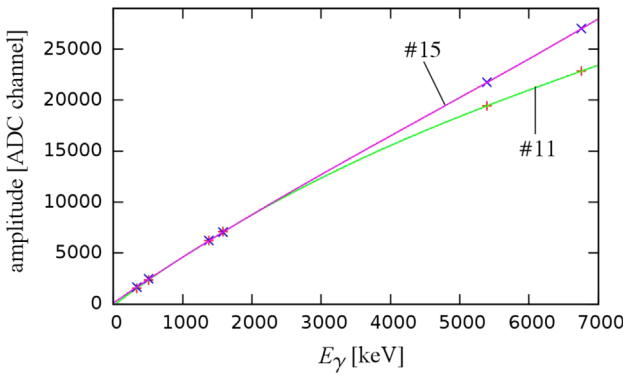

Fig. 3. The energy response of the LaBr$_3$(Ce) plus Hamamatsu R9779 PMT detector assembly exhibits an onset of non-linearity at about 3 MeV with detector dependent non-linearity. The energy is calibrated using a third order polynomial.

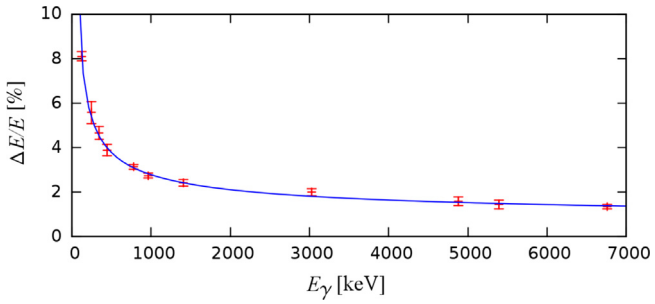

Fig. 4. The $LaBr_3$(Ce)-FATIMA relative energy resolution corresponding to FWHM/E_γ. The calibration function is proportional to $1/\sqrt{\alpha+E_\gamma}$ with α being related to the PMT gain variance [18].

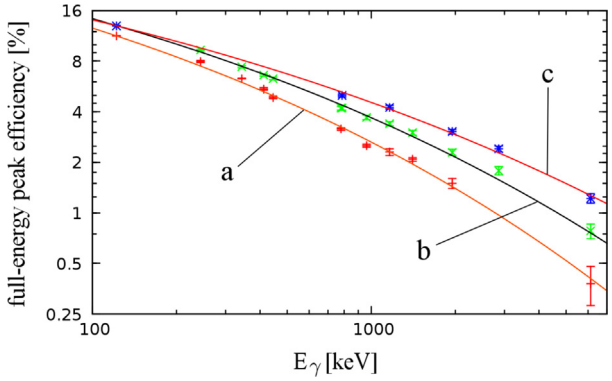

Fig. 5. The absolute full-energy peak efficiency curves of (a) the FATIMA set-up, (b) the EXILL array and (c) the EXILL array including add-back algorithm.

derived using the relative intensities reported in Ref. [19]. The resulting relative efficiency curve then was normalised to the absolute efficiency curve obtained from the ^{152}Eu source. In Fig. 5a, the full-energy peak efficiency of the FATIMA set-up (superposition of 16 $LaBr_3$ spectra) is compared with the EXILL efficiency (superposition of 32 Ge spectra) and the EXILL efficiency including add-back events. Additional efficiencies for 1333 keV have been measured using a ^{60}Co γ-ray source with activity of 193 kBq. Precise values, also for single detectors, are given for specific energies in Table 1.

As Ge–$LaBr_3$–$LaBr_3$ or Ge–Ge–$LaBr_3$–$LaBr_3$ coincidences often need to be used, the efficiency of the EXILL array should not be smaller than the efficiency of the FATIMA set-up. In our case, the EXILL array is more efficient than FATIMA. When add-back is enabled, the increase of the EXILL efficiency sets in already at about 400 keV and is, at 6.1 MeV, about 56% larger than the case where add-back is disabled.

2.5. *Background considerations*

Typical background obtained in γ-ray spectroscopy is most unwelcome in fast-timing experiments using γ rays. Considering energies larger than 300 keV, the background underneath the full-energy peak consists predominantly of Compton-scattered events. In this case, a Compton-timing correction for lifetime determination using a straightforward procedure can be performed, as will be demonstrated in Section 3. However, any correction procedure introduces additional errors which in turn reduce the accuracy of the lifetime determination. Below 300 keV, the Compton background becomes important when many γ rays are produced, as it then results from the superposition of many Compton continua of γ rays of higher energies. In addition, scattered γ rays can contaminate the γ-ray spectrum, in particular the back-scatter

Table 1
The absolute full-energy peak efficiencies $\epsilon(E_\gamma)$ of the different components of the mixed EXILL&FATIMA spectrometer, where E_γ is given in units of keV. The efficiencies for 122, 1333 and 6111 keV were obtained as described in the text. The values for the ^{137}Cs energy of 662 keV were interpolated from the efficiency curves as presented in Fig. 5.

Detector (array)	ϵ(122) (%)	ϵ(662) (%)	ϵ(1333) (%)	ϵ(6111) (%)
FATIMA	11.31(6)	3.71(7)	2.05(6)	0.38(10)
EXILL[a]	12.98(6)	4.92(5)	2.97(4)	0.78(8)
EXILL[a]+add-back	13.01(6)	5.80(5)	3.81(5)	1.22(11)
Ge crystal at 14.5 cm	0.41(1)	0.154(6)	0.093(3)	0.024(1)
1.5 in. long $LaBr_3$ at 8.5 cm	0.71(1)	0.21(1)	0.109(5)	0.020(6)
2 in. long $LaBr_3$ at 8.5 cm	0.70(1)	0.25(1)	0.145(6)	0.028(7)

[a] EXILL configuration with 32 Ge crystals in combination with FATIMA.

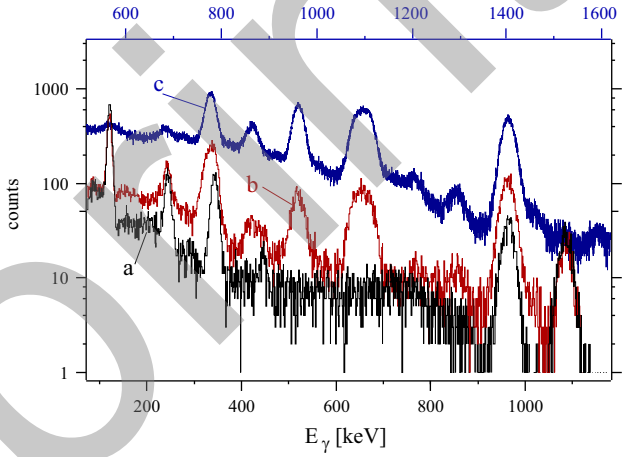

Fig. 6. The effect of cross-talk events [spectrum (b)]: The $LaBr_3$(Ce) detector number 1 coincidence spectra obtained with a gate on the 444-keV transition in ^{152}Sm using (a) a non-neighbouring $LaBr_3$(Ce) detector and (b) a directly neighbouring $LaBr_3$(Ce) detector. Spectrum (c) is the singles energy spectrum as obtained using the ^{152}Eu source, that is shifted by −444 keV for comparison.

peaks around 200 keV. Such scattered γ-ray events are produced by a Compton scattering of an initial γ ray in the surrounding material of the set-up including the other detectors and the Compton-scattered γ ray then is detected. An active Compton suppression, for instance by using BGO scintillators, also acts as an active shield for $LaBr_3$ detectors, reducing remarkably events resulting from scattered γ rays [20]. A simple estimate of the solid angle indicates that the $LaBr_3$–$LaBr_3$ coincidence efficiency would drop by a factor of 2 if the distance of the $LaBr_3$ detectors was increased by only 2 cm, the distance necessary to install efficient shielding. Therefore, we dispensed with the use of any active or passive $LaBr_3$-detector shielding.

We performed an investigation of the possible effect of scattered γ rays by generating gated spectra of pure $LaBr_3$–$LaBr_3$ double events (γ-ray multiplicity equal to 2) for different detector combinations (i,j) with $j>i$, as illustrated in Fig. 6. By combining an $LaBr_3$ detector located on one side of the central EXOGAM-clover ring with an $LaBr_3$ detector located on the opposite side of the central ring [e.g. for combination (1,9)] the expected gated $LaBr_3$ coincidence spectrum with almost Gaussian shaped full-energy peaks is observed. The corresponding $LaBr_3$ coincidence spectrum (a) of Fig. 6 was generated by using an $LaBr_3$ gate on the 444-keV transition in ^{152}Sm, as obtained using the ^{152}Eu source. Note also the almost constant Compton continuum of the 964-keV transition and the constant increase of the Compton background for energies below the other full-energy peaks. ^{152}Eu partially decays to excited states in ^{152}Sm via electron-capture decay

(72.1% [21]) and states in ^{152}Gd via β^- decay. The 444-keV transition in ^{152}Sm is a doublet with coincident transitions of 122, 244, 964 and 1085 keV. The ^{152}Gd peak at 344 keV is due to accidental coincidences with the Compton background underneath the 444-keV peak (see also Fig. 2a). Unsurprisingly, the central EXOGAM-clover ring serves as an effective passive shield. The dramatic effect of scattered γ rays coming from directly neighbouring $LaBr_3$ detectors is illustrated by spectrum (b) of Fig. 6. Using the same $LaBr_3$ gate at 444 keV, the resulting coincidence spectrum of the directly neighbouring $LaBr_3$ detector is full of "ghost peaks" which are overlapping with the transitions of interest. By comparing spectrum (b) with spectrum (c), the superimposed structure seen in spectrum (b) corresponds to the singles energy spectrum of the ^{152}Eu source which is shifted by exactly -444 keV, corresponding to the energy of the $LaBr_3$ gate. This clearly indicates that an initial γ ray depositing energy from a Compton-scattered event in one detector and the Compton-escaped γ ray being absorbed by the neighbouring detector. This therefore provides a false γ–γ coincidence, often called a "cross-talk event" with a false timing information related to the time-of-flight of the Compton-scattered γ ray. Fortunately, such undesired cross-talk events are only observed in adjacent $LaBr_3$-detector combinations. The detector combinations (i,j) with $j > i+1$ all show identical clean coincidence spectra as the spectrum (a) as shown in Fig. 6. One can say that the combinations (i,j) with $j > i+1$ within a ring are passively shielded by the detectors $i+1$. While add-back is straightforward, there is no simple algorithm that could take into account the time information of the initial γ ray, since corrections would introduce additional errors. Instead, we refrained from using detector combinations (i,j) with $j = i+1$ within the $LaBr_3$ rings for further analysis. In this way, the excluded detector combinations (i,j) with $j = i+1$ partially act as an active shield for combinations with $j \geq i+2$ and thus also the Compton background in both $LaBr_3$ spectra i and $j \geq i+2$ is reduced. In total, 16 detector combinations out of 120 are excluded from the analysis, corresponding to a relative loss of about 13% in statistics.

An advantage of fast timing with $LaBr_3$(Ce)-scintillator detectors is that they offer good energy resolution allowing for clean selection of γ lines. Still, when the γ-ray spectrum is complex such as those in our experiments, the energy resolution may not be sufficient to disentangle the transition of interest amidst other γ lines. Our experiment has been specifically designed to allow for cascade selection by exploiting the high-resolution Ge detectors of the EXILL array. In this way, a γ ray of a subsequent triple γ-ray cascade is selected as a trigger [22]. Beside the possible exclusion of unwanted contaminating γ rays from other cascades or nuclei, this procedure improves the peak-to-background ratio remarkably due to suppression of most of the γ rays that are shown in the singles spectra, as can be seen in Fig. 7. The higher the energy of the EXILL triggering transition, the more effective is the Compton-background reduction observed in the doubly gated (Ge+$LaBr_3$) $LaBr_3$ coincidence spectra. In a de-excitation pattern with multiplicity 3, the resulting doubly gated $LaBr_3$ spectrum often shows the spectrum of a single γ ray with virtually no Compton background, as shown in Fig. 7.

2.6. γ–γ timing performance of FATIMA

To be able to exploit lifetimes down to values corresponding to the intrinsic timing resolution of any γ–γ fast-timing set-up, the time response of the set-up as a function of the energy of prompt γ–γ cascades, or "prompt response functions" (PRF), needs to be determined. The time response, defined by the centroid of the PRF, represents the zero-time t_0 relative to the physical prompt reference and needs to be measured using different γ–γ cascades.

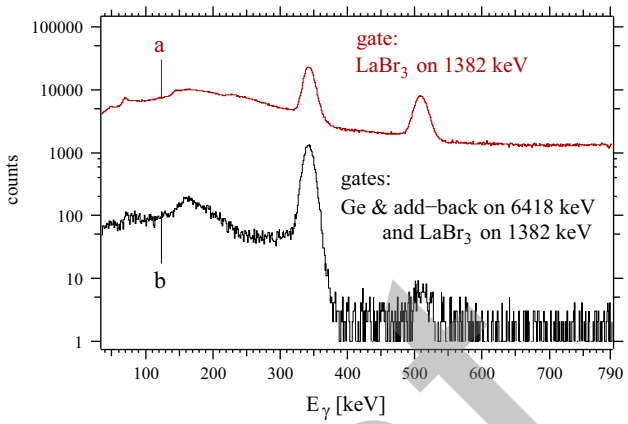

Fig. 7. Improvement of the peak-to-background ratio by using a high-resolution EXILL gate. (a) In-beam $LaBr_3$(Ce) coincidence spectrum of double events in ^{49}Ti obtained using an $LaBr_3$ gate at 1382 keV. (b) By using triple events and an additional EXILL gate at 6418 keV, the Compton background underneath the 342-keV peak is almost totally suppressed due to elimination of higher energy γ rays.

The PRF corresponds to the time spectrum which is obtained for lifetimes $\tau \lesssim 1$ ps and the FWHM of the approximately symmetric PRF provides an estimate of the absolute time resolving power of the γ–γ set-up according to [23]

$$\delta t = \frac{\mathrm{FWHM}}{2\sqrt{2\ln 2}\sqrt{n}}, \tag{1}$$

where n is the number of events of which the PRF is built up. Assuming no background contributions, a "delayed" time spectrum is measured as the convolution of the PRF $P(t)$ with an exponential decay [23]:

$$D(t) = n\lambda \int_{-\infty}^{t} P(t'-t_0)e^{-\lambda(t-t')}\,dt' \quad \text{with } \lambda = 1/\tau, \tag{2}$$

where λ is the transition probability and τ is the mean lifetime of the nuclear excited state interconnected by the γ–γ cascade and t_0 is the centroid of the PRF. For lifetimes which are larger than the FWHM of the PRF, the slope method is used by fitting the straight line observed in the semi-logarithmic plot of $D(t)$ outside the region of the PRF, as $\ln[D(t)] = -\lambda t$ for $t \gg t_0$. The slope method is independent of the shape of the PRF [23].

Assuming no background contributions, the method to measure lifetimes with highest precision is the centroid-shift method [24]. The centroid or centre of gravity is the first moment of the statistical distribution and for an arbitrary time spectrum $D(t)$ is defined as

$$C^D = \langle t \rangle = \frac{\int_{-\infty}^{\infty} tD(t)\,dt}{\int_{-\infty}^{\infty} D(t)\,dt}, \quad \delta C^D = \sqrt{\langle t^2 \rangle - \langle t \rangle^2}. \tag{3}$$

For a symmetric Gaussian PRF, the statistical uncertainty of the centroid determination δC^P is equal to δt from Eq. (1). Basically and assuming no background contributions, the mean lifetime directly corresponds to the relative time difference between the centroids of the delayed time spectrum and the energy corresponding PRF as [24]

$$\tau = \pm [C^D - C^P], \tag{4}$$

where the sign is negative if the decay transition of the γ–γ cascade provides the start signal to the TAC ("the anti-delayed time spectrum" [23]). As demonstrated experimentally in Refs. [25,26], the centroid-shift method is independent of the shape of the PRF.

Considering specific detector combinations, one generally observes small differences of the decisive FWHM of the PRF dependent on the detector combination. According to the Hyman

theory of timing [27], the time resolution of a scintillator plus PMT detector assembly is proportional to the figure of merit $\sqrt{\tau_{sc.}/N_{pe.}}$, where $\tau_{sc.}$ is the scintillator decay time and $N_{pe.}$ is the number of photoelectrons produced at the photo cathode of the PMT by the scintillation light pulse. Thus, the timing is controlled by the scintillator light output and the PMT photo-cathode sensitivity [28,29]. Using large volume scintillators ($>$ ⌀0.5 in. $\times$ 0.5 in.), the time spread of the scintillation light collection at the PMT photo cathode dominates over the PMT time jitter (transit time spread of photoelectrons) [30,31]. We measured the FWHM to be 210–240 ps when combining two "small" $LaBr_3$ scintillators (⌀1.5 in. $\times$ 1.5 in.) using a ^{60}Co source (1173–1333-keV cascade with $\tau = 1.06(3)$ ps [32]). By combining two large scintillators (⌀1.5 in. $\times$ 2 in.), the result is 260–300 ps. The small differences of the FWHM for combinations of equal volume detectors may be associated with a spread in the quality of the crystals due to variation of Ce doping [33]. Small variations of the CFD adjustments (CFD shaping delay, threshold and walk) can also slightly affect the FWHM [26]. An additional detector combination dependent electronic time jitter is given due to cable-length dependent degradation of the signal-to-noise ratio and the generation of additional noise by the individual electronic modules of the fast-timing circuitry [15]. The most important factor overall in this experiment is the FATIMA timing performance, which is obtained by a superposition of the $N(N-1)/2$ calibrated"$TAC_{(i,j)}$" time spectra. To provide the best FATIMA timing performance, only an alignment of the calibrated $TAC_{(i,j)}$ spectra needs to be applied to the raw data by using error-free constant-shift values "$shift_{(i,j)}$" (implemented in SOCOv2 [17]). The precise $shift_{(i,j)}$ constants were derived from the measurement of the "stop" centroid C_{stop} of each single $TAC_{(i,j)}$ time spectrum of a specific γ–γ cascade. The FATIMA PRFs presented in Fig. 8 represent the TAC-aligned and superimposed FATIMA "stop" time spectra as obtained when the decay transition was registered by detectors which provided the stop signals to the TACs of the set-up.

As a result of statistical processes in the creation of the detector output pulse, the FWHM of the PRF is dependent on the γ-ray energy of both the feeding (start signal) and the decaying (stop signal) transitions. The main component is induced when the signals have smaller amplitude (energy), as the relative amplitude variation (jitter) increases with decreasing amplitudes [35]. At very high energies, as the case presented in Fig. 8b, the relative amplitude variation is marginal and the FWHM is dominated by the crystal-size dependent time spread of the scintillation light collection. For energies larger than 1.2 MeV, the FWHM of the combined FATIMA PRF is 270(20) ps. The energy dependent FATIMA timing performance is presented in Fig. 9, where the data are fitted using a function $\Delta T(E)$ which describes the CFD timing uncertainty and time walk according to [26,35]

$$\Delta T(E) = \frac{a}{\sqrt{E+b}} + \mathrm{pol}(E), \tag{5}$$

where pol(E) is a polynomial of order n. In our case, the best fit was obtained for pol(E) being a constant which is expected for a linear energy response [26]. According to Eq. (1) and assuming only 1000 events in a PRF with no background contribution, the statistical uncertainty of the PRF-centroid determination is less than 5 ps for energies larger than 300 keV.

In analogy to a simple two detector γ–γ timing system, it is very important to distinguish between the "start" and the "stop" time spectrum, as the electronic timing uncertainty (time-jitter) of the start and stop signals are, in general, different (the so-called "timing asymmetry" [26]) and provoke asymmetric semi-Gaussian prompt time spectra (PRFs). As illustrated in Fig. 10a, neither the start and stop time spectra, nor the shift of both time spectra relative to the reference zero-time are mirror symmetric. In this

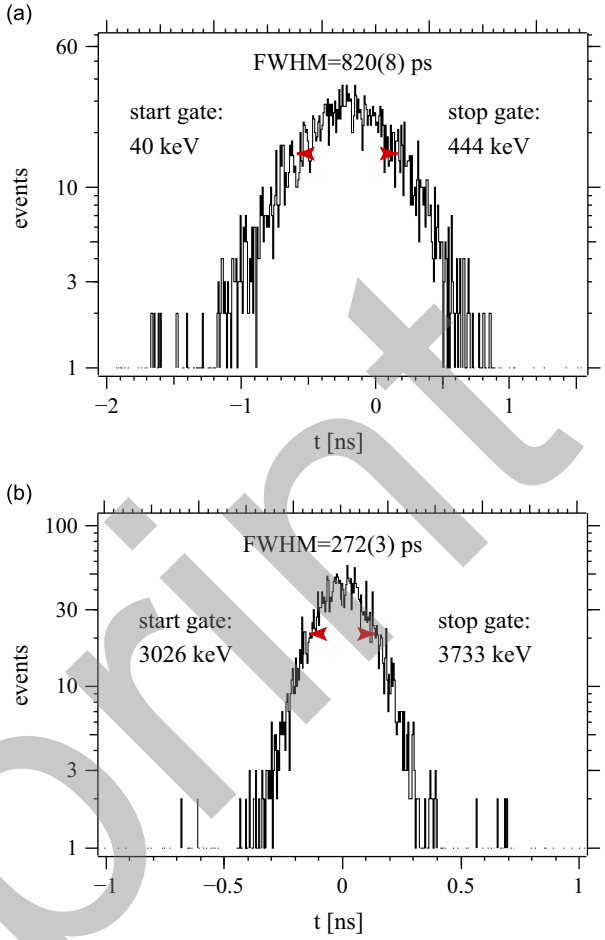

Fig. 8. The experimental FATIMA prompt time spectra (PRFs). (a) PRF obtained using triple Ge–$LaBr_3$–$LaBr_3$ events by gating the $LaBr_3$-start detectors on the 40-keV Sm K–X ray which is prompt relative to the electron capture decay of ^{152}Eu and the $LaBr_3$-stop detectors on the 444-keV decay transition in ^{152}Sm ($\tau < 1$ ps [21]) and an additional clover add-back gate on the following 1085-keV ground-state transition. (b) PRF obtained using double $LaBr_3$–$LaBr_3$ events of the ^{48}Ti(n_{th}, γ)^{49}Ti reaction ($\tau < 20$ fs [34]). No background contribution is given in this case, as no further coincident γ rays are present for $E_\gamma > 3$ MeV.

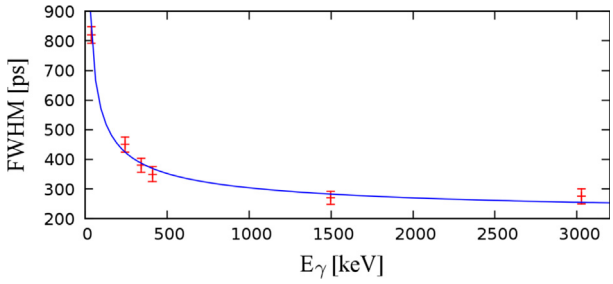

Fig. 9. The FATIMA γ–γ timing performance expressed as the FWHM of FATIMA PRFs. The absolute statistical timing resolution is given by Eq. (1). The energy of the data points corresponds to the smaller energy of the two γ rays of the γ–γ cascade. Each error bar represents the statistical uncertainty plus 20 ps to account for the small difference of the electronic time-jitter of the larger energy with $E_{large} > 440$ keV.

case, the timing asymmetry arises from the disparities of the individual detector time responses (time walk) as a result of the different energy responses observed for large energy differences $|\Delta E_\gamma| = |E_{feeder} - E_{decay}| > 3$ MeV (see also Fig. 3). But in spite of this fact, the centroid difference, that is the time shift between the centroids of the stop and start time spectra for a specific γ–γ cascade, is independent of any timing asymmetry [15,26,36]. This

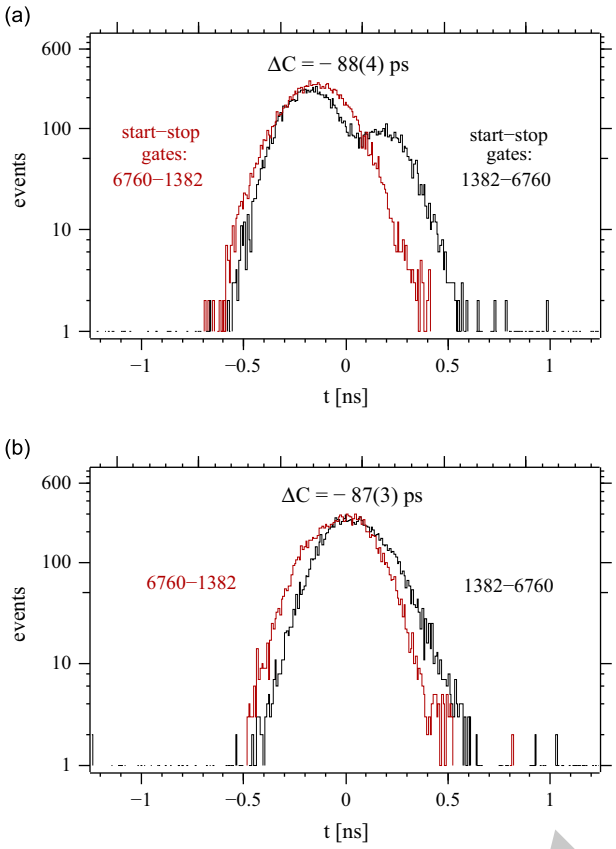

Fig. 10. Illustration of the PRD constancy. (a) The two independent start and stop semi-Gaussian FATIMA PRFs of the 6760–1382-keV cascade in ^{49}Ti ($\tau = 4.9(6)$ ps [34]), as obtained using the derived shift$_{(i,j)}$ constants. (b) The same data as in (a) treated using other shift$_{(i,j)}$ constants to improve the timing performance (FWHM = 305(6) ps).

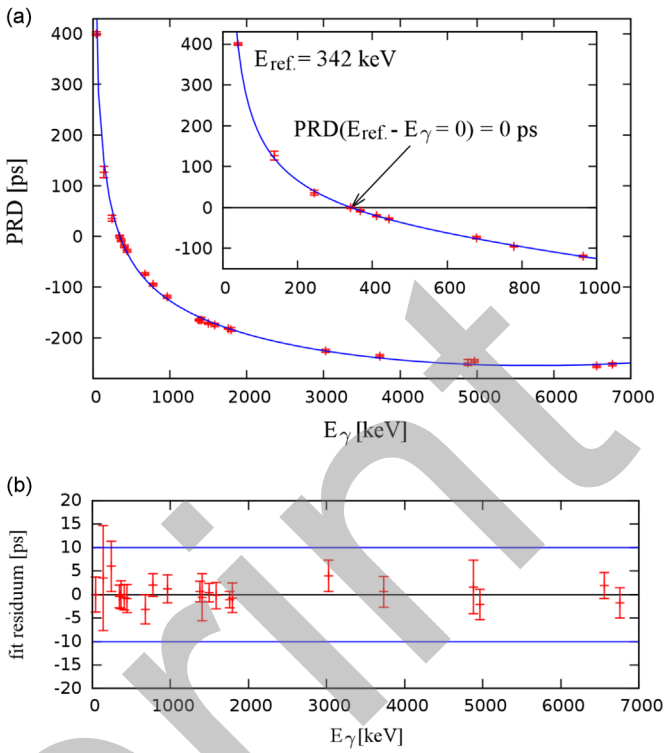

Fig. 11. (a) The energy dependent FATIMA mean prompt response difference (PRD) for prompt full-energy γ–γ timing between the start and stop events recorded by the FATIMA set-up. The data are adjusted for the reference energy of 342 keV, as explained in the text. The inset shows the time response for the low energy region, where the PRD curve crosses the energy axis at the reference energy, according to Eq. (7). (b) The PRD fit residuum of the calibration function given by Eq. (5) with indicated overall PRD-calibration uncertainty of 10 ps.

is illustrated in Fig. 10, which also shows that the applied shift$_{(i,j)}$ constants do not introduce systematic errors. While the centroid difference is unchanged for different constants, the precision of the measurement can be improved following Eq. (1) by minimising the FWHM.

The advantage of the generalised centroid difference (GCD) method is that the centroid difference is mirror symmetric [36]. By referring to the decay transition and according to Eq. (4), the following relation is strictly valid:

$$\Delta C(\Delta E_\gamma)_{\text{decay}} = C^D_{\text{stop}} - C^D_{\text{start}} = \text{PRD}(\Delta E_\gamma)_{\text{decay}} + 2\tau \qquad (6)$$

with $\Delta E_\gamma = E_{\text{feeder}} - E_{\text{decay}}$. $\text{PRD} = C^P_{\text{stop}} - C^P_{\text{start}}$ is the prompt response difference and represents the linearly combined γ–γ time response (time walk) of the complete fast-timing system (the measured PRD mathematically corresponds to the mean value $\overline{\text{PRD}}$ for $N > 2$ [15] and is hereafter not indicated). C^D_{stop} (C^D_{start}) is the centroid of the time spectrum which is obtained for the reference energy, the decay energy in Eq. (6), being the energy of the stop (start) gate. The mirror symmetric centroid difference makes it possible to precisely calibrate the energy dependency of the PRD. For any energy combination of a prompt γ–γ cascade, two data points with the same uncertainty are obtained by taking advantage of the GCD identity $\text{PRD}(\Delta E_\gamma = 0) = 0$. The two data points are transformed into the $(\Delta C, E_\gamma)$−representation according to [15,26]

$$\text{PRD}(E_{\text{feeder}} - E_{\text{decay}}) = \text{PRD}(E_{\text{feeder}}) - \text{PRD}(E_{\text{decay}}). \qquad (7)$$

According to Eq. (6), also precisely known ps lifetimes can be used for the PRD-calibration procedure, as described in more detail in Ref. [26]. The PRD curve of the FATIMA set-up, presented in Fig. 11a, was obtained by adjusting the two data points of 16 γ–γ cascades in parallel to fit the smoothest PRD curve. Some 82% of the PRD data were obtained using triple events (multiplicity 3) with an additional EXILL gate which resulted in almost zero background contributions, as the case presented in Fig. 7. Triple γ–γ–γ events were used from a 40-hour measurement using a ^{152}Eu point like γ-ray source for the energy range of 40–1408 keV and from a 20-hour measurement using the ^{48}Ti(n$_{\text{th}}$, γ)^{49}Ti reaction for the energy range of 137–6760 keV. The rest of the PRD data are from double events, where γ–γ cascades were used which provided peak-to-background ratios larger than 20. No significant timing effects due to the background contributions were found in these cases. The PRD data are fitted by a function according to Eq. (5) with a second order polynomial. The quality of the PRD calibration is represented by the deviations of the data from the fit, as shown in Fig. 11b. By taking statistical uncertainties into account, an overall PRD uncertainty of 10 ps is achieved. No further error is given by this PRD-calibration procedure, as no corrections have been applied to the raw data. Although the metallic Ti target had a surface area of about 40 mm^2, the results are consistent with the ^{152}Eu data in the overlapping energy region of 137–1408 keV.

Measurements have been performed to test the long-term stability of the set-up by means of two further 3-hour calibration of the PRD using the ^{152}Eu source. As illustrated in Fig. 12a, the 3 measurements were separated over the fast-timing campaign of 5 weeks. Compared with the PRD uncertainty of 10 ps, no significant change of the PRD characteristics in the low-energy region of 40–1408 keV can be observed. Additional PRDs were measured using an extended ^{60}Co source with a diameter of 10 mm and the superimposed data of several 1-hour high-energy-calibration measurements using double events from a

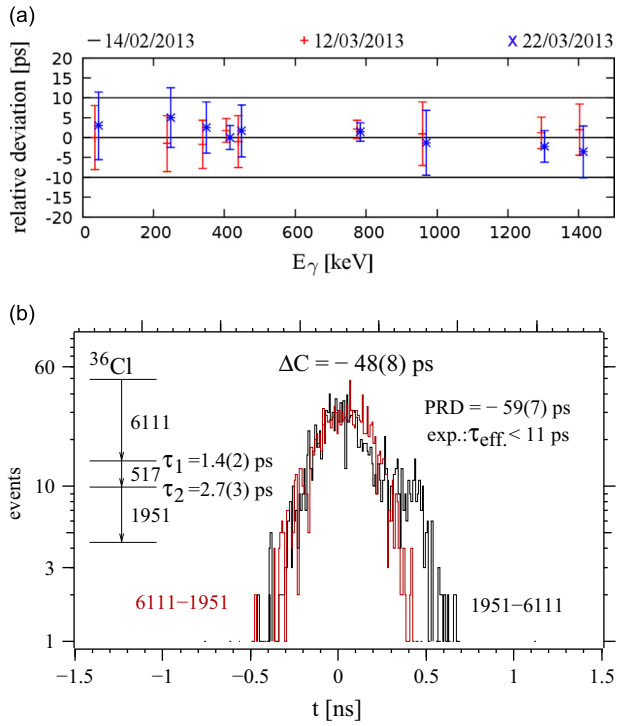

Fig. 12. (a) The relative deviations of three low-energy PRD-calibration measurements using a ^{152}Eu point-like γ-ray source compared with the overall PRD uncertainty. The first calibration is represented by the zero-line. (b) The superimposed data of the 6111–1951-keV cascade in ^{36}Cl obtained using the data of four 1-hour measurements which were separated by several days within 2 weeks. Each time spectrum is built with about 1500 events. The derivation of the result is explained in the text. The literature values τ_1 and τ_2 are taken from Ref. [37].

^{35}Cl(n_{th}, γ)^{36}Cl reaction for the almost prompt indirect 6111–1951-keV γ–γ cascade. In the case presented in Fig. 12b, the effective lifetime obtained corresponds to $\tau_{eff.} = \tau_1 + \tau_2$ [25]. If τ_1 is known, τ_2 can also be derived in this way, which can provide a more precise result when the spectrum of the direct feeding transition has a γ-ray contamination or has a bad peak-to-background ratio. Within statistical uncertainties, the results are consistent with Eq. (7) using the PRD curve presented in Fig. 11a. As the dimensions of the sources and targets were different and also their positions in the spectrometer to within about 2 mm, the results also indicate that the use of a 3-dimensional centrally symmetric FATIMA set-up in combination with the GCD method reduces geometrical timing effects to an unmeasurable value in our case.

3. Tests on the ^{235}U fission experiment

In (n_{th},γ) experiments, the use of a high-resolution energy gate using Ge detectors as a coincidence trigger provides a considerable Compton-background reduction which is important for γ–γ fast-timing measurements. Owing to the low γ-ray multiplicity of these type of reactions, the doubly gated (Ge+$LaBr_3$) $LaBr_3$ coincidence spectrum often contains only one γ ray, and virtually no background is underneath the full-energy peak, as illustrated in Fig. 7. If this is the case for both the feeding and the decay transitions, the resulting $LaBr_3$–$LaBr_3$ time spectrum is free of background. In the most general situation one has to deal with Compton-background contributions, and in particular in prompt fission experiments, where the γ-ray multiplicity is much higher and the amount of γ lines is increased by a factor of 100 or more compared to relatively clean (n_{th},γ) experiments. By using two high-resolution Ge gates, a clean spectrum of one γ line can be

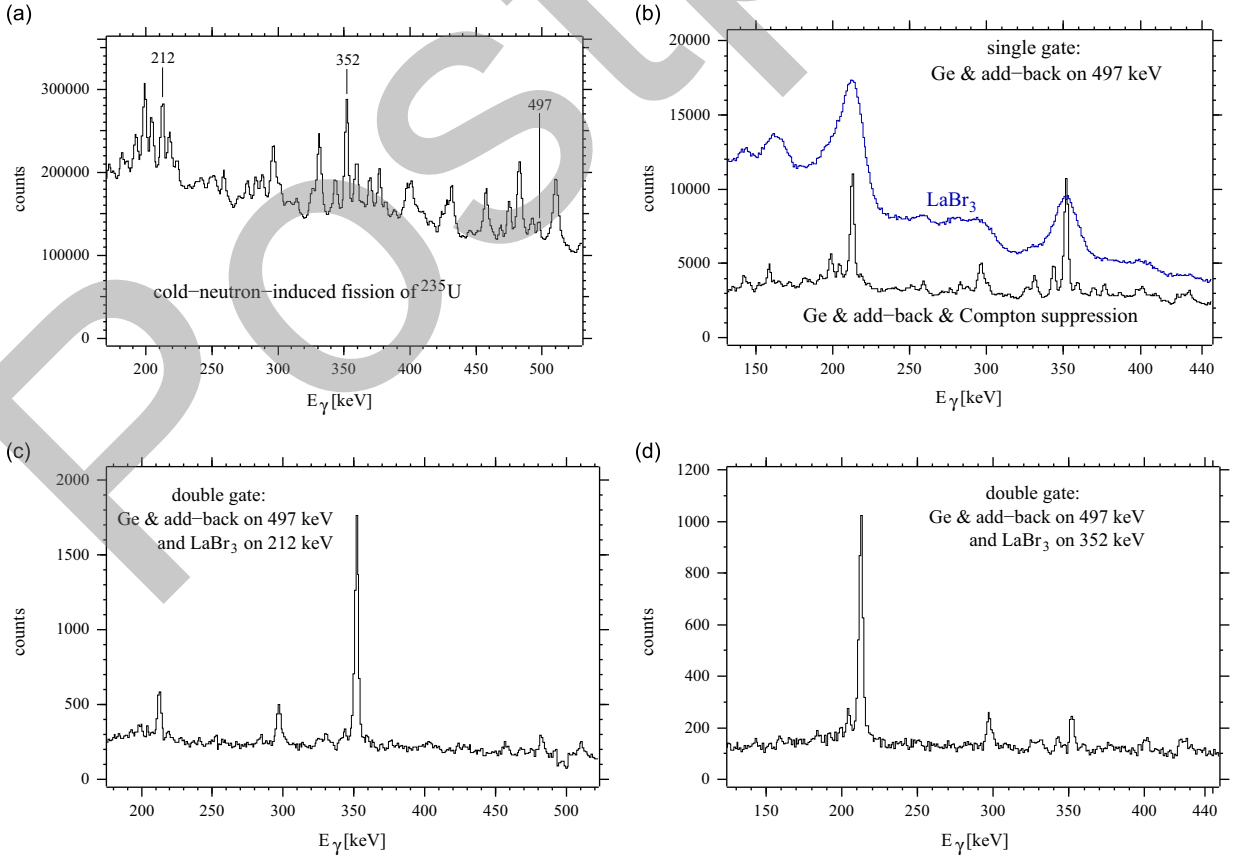

Fig. 13. (a) The total (no gate) EXILL projection of triple events in fission fragments following neutron-induced fission of ^{235}U with γ rays of ^{100}Zr. (b) The FATIMA and EXILL projection of triple events obtained using an EXILL gate (Ge plus add-back) on the 497 keV $6^+ \rightarrow 4^+$ transition in ^{100}Zr. (c) Doubly gated EXILL spectrum of the 352-keV $4^+ \rightarrow 2^+$ transition obtained using gates as indicated. (d) Doubly gated EXILL spectrum of the 212-keV $2^+ \rightarrow 0^+$ ground-state transition.

obtained, but at the expense of much reduced statistics, since the probability to record multiplicity 4 events is about 1–5% of the triple efficiency. Also the relative γ-ray intensity ratio within a selected quadruple γ-ray cascade can be reduced.

For the purpose of investigating the timing effect of the Compton background, two results of the cold-neutron-induced fission experiment on ^{235}U are presented. This experiment delivered the highest count rates during the EXILL&FATIMA campaign with about 10 kHz for a single Ge crystal and 15 kHz for an $LaBr_3$ detector. A data rate of about 6.5 MB/s was created by the 71 channels of the EXILL&FATIMA spectrometer. The target consisted of 0.8 mg $^{235}UO_2$ tightly sandwiched with cyanoacrylate between two 15−μm thick Be backings in order to stop the neutron-induced fission fragments within the target. The analysis was performed using multiplicity 3 events out of 0.8 TB of data, corresponding to a tenth of the acquired data. The total projection of the EXILL array including add-back and BGO Compton suppression is shown in Fig. 13a. The transitions labelled belong to the nucleus ^{100}Zr which has a fission yield of 4.98%, close to the maximum value. Fig. 13b shows the comparison of the EXILL and FATIMA projections of triple events generated by using a clover add-back gate on the 497-keV $6^+ \rightarrow 4^+$ transition. The two spectra show similar structures with expected strong peaks at 352 keV and 212 keV. Since the introduced Compton suppression of the $LaBr_3$ detectors geometrically does not fully cover the $LaBr_3$ crystals, the peak-to-background ratio of the FATIMA projection is slightly worse. The small peaks identified in the EXILL projection can be due to true coincidences, e.g. with a γ ray from a state above the 6^+ state, or from a double γ-ray cascade in another nucleus. The doubly gated EXILL spectrum of the 352-keV $4^+ \rightarrow 2^+$ transition presented in Fig. 13c was obtained using a clover add-back gate on the 497-keV transition and a 10-keV-wide $LaBr_3$ gate centred on the 212 keV $2^+ \rightarrow 0^+$ ground-state transition. This high-resolution spectrum allows investigations of possible coincident γ rays in the vicinity (±20 keV, dependent on the energy range) of the 352-keV transition. A similar investigation of the 212-keV ground-state transition is shown in Fig. 13d. In both cases, no significant full-energy peak is observed in the vicinity of the transitions of interest using Ge+$LaBr_3$ gated spectra of triple events. Thus the lifetime of the first 2^+ state can be measured using Ge–$LaBr_3$–$LaBr_3$ coincidences, and only Compton background will additionally contribute to the time spectra.

Fig. 14a shows a doubly gated FATIMA $LaBr_3$ spectrum of the feeding transition at 352 keV ($LaBr_3$ energy projection of the Ge+$LaBr_3$ gated fast-timing matrix). A large Compton background is observed, the peak-to-background ratio as obtained for the energy width corresponding to the width of the $LaBr_3$ gate is 2.5 (2). Thus about 40% of the events in the EXILL-gated γ–γ time spectra shown in Fig. 14b are background events (e.g. full-energy vs. Compton and Compton vs. Compton). The two start and stop time spectra show a pronounced decay slope from which the lifetime can be extracted assuming the background time distribution to be nearly prompt. This assumption is safe, since the centroid difference is much smaller than 2τ; the PRD for the energy combination 352–212 keV is only −62(10) ps. The measurement by means of the slope method results to a mean lifetime of 720(40) ps.

To obtain the lifetime from the centroid shift, the time response or "timing" (centroid of time spectrum) of the background underneath the full-energy peak has to be taken into account, in order to perform the Compton-timing correction [6,25] to remove its contributions from the time spectrum as shown in Fig. 14b. Obviously, the time spectrum of the background events at 352 keV cannot be measured directly. However, the timing of the Compton background underneath the full-energy peak at 352 keV can be extrapolated precisely. The two (start and stop) fast-timing

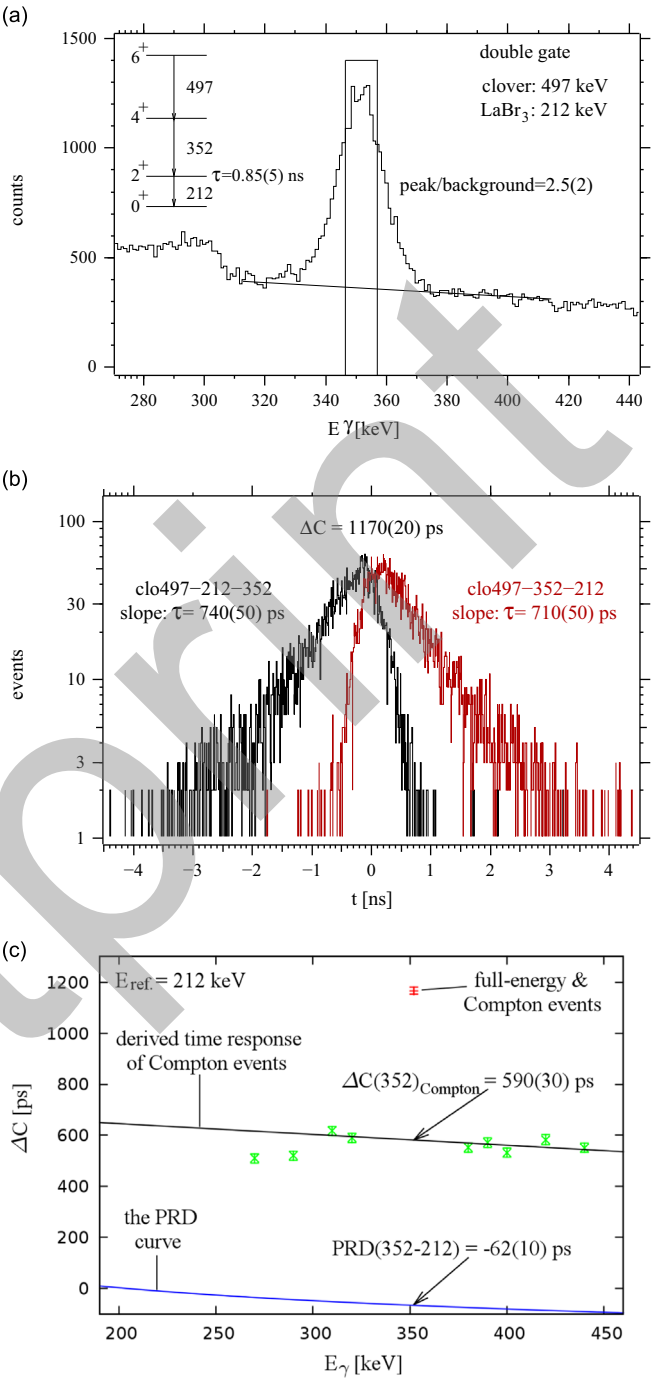

Fig. 14. (a) Doubly gated (Ge+$LaBr_3$) FATIMA γ-ray spectrum. The literature value indicated for the lifetime of the first 2^+ state in ^{100}Zr is taken from Ref. [38]. (b) The two EXILL-gated FATIMA time spectra of the $4^+ \rightarrow 2^+ \rightarrow 0^+$ cascade in ^{100}Zr with about 5900 events each. (c) Illustration of the Compton-background time-correction procedure by the centroid difference diagram for the reference energy of 212 keV (common gate of all time spectra). Details are discussed in the text.

matrices allow for a quick background analysis by generating a set of time spectra using gates set in the Compton background around the full-energy peak. For proper time correction, the energy width of the Compton gates need to correspond to the width of the full-energy gate. The result of the Compton-background analysis on the 352-keV feeding transition is presented in Fig. 14c, where the indicated PRD curve PRD (E_γ) is adjusted for the reference energy of 212 keV (parallel shift of the PRD curve in order to cross the energy axis at 212 keV). The Compton-background events are largely delayed which is partially due to the lifetime of the

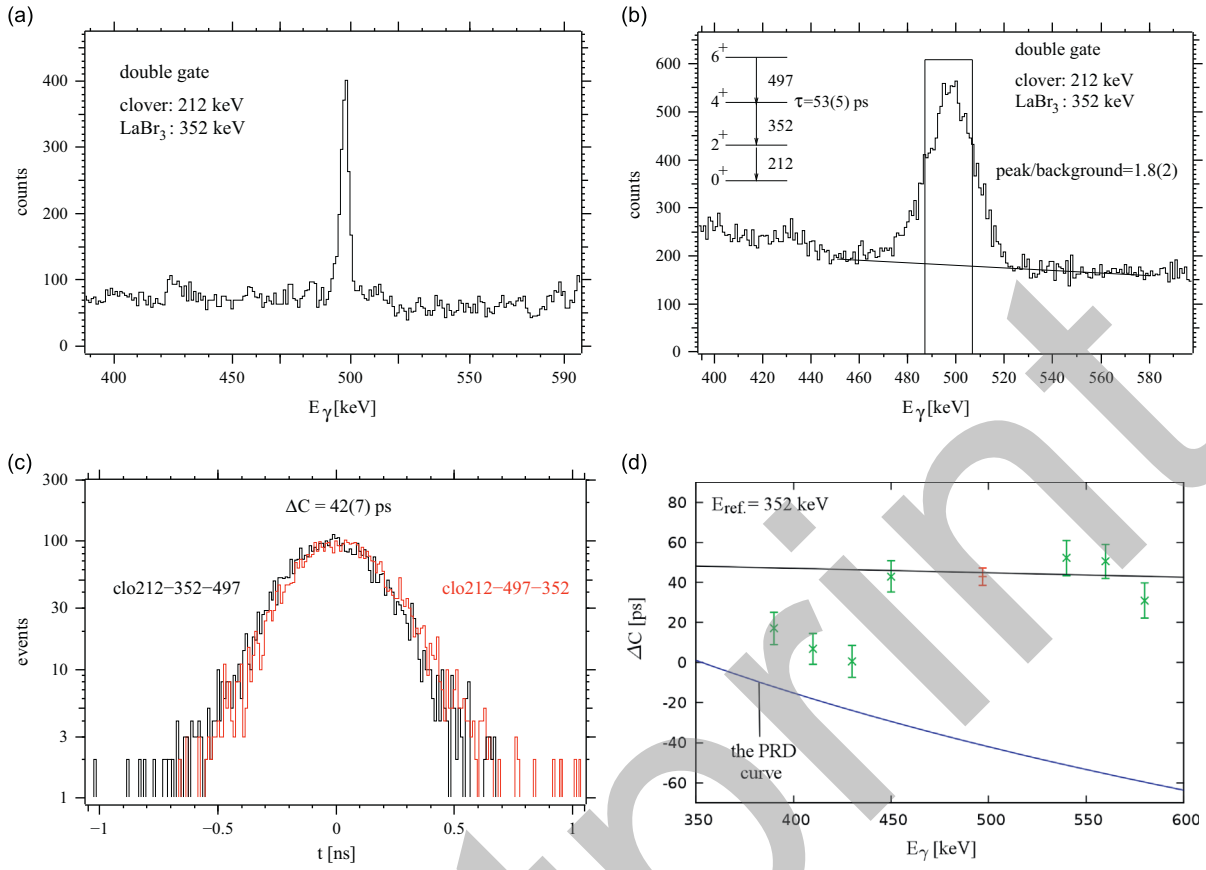

Fig. 15. (a) Doubly gated EXILL spectrum obtained using gates as indicated to investigate for unwanted γ rays close to the 497-keV γ-ray line. (b) Doubly gated FATIMA γ-ray spectrum with inset indicating the literature value of the lifetime of the first 4^+ state in ^{100}Zr [38]. (c) The two EXILL-gated FATIMA time spectra of the $6^+ \rightarrow 4^+ \rightarrow 2^+$ cascade in ^{100}Zr with about 4600 events each. (d) Compton-background analysis using the centroid difference diagram for the reference energy of 352 keV. At 497 keV, the PRD is −42(10) ps.

2^+ state decaying via the 212-keV γ ray which was used to generate the time spectra. As illustrated in Fig. 14c, the time response of the Compton background as a function of the energy is smooth for $E_{\mathrm{Compton}} > 300$ keV. The interpolation of the Compton-background centroid difference at 352 keV using a linear function for $E_{\mathrm{Compton}} > 300$ keV yields a result of $\Delta C_{\mathrm{Compton}} = 590(30)$ ps. The lifetime using the centroid shift methods is derived as a linear combination of centroids, the measured centroid difference corresponds to [36]

$$\Delta C = \frac{\Pi \Delta C_{\mathrm{true}} + \Delta C_{\mathrm{Compton}}}{1+\Pi} \tag{8}$$

where Π is the peak-to-background ratio and ΔC_{true} is the true centroid difference. It follows:

$$\Delta C_{\mathrm{true}} = \Delta C + \frac{\Delta C - \Delta C_{\mathrm{Compton}}}{\Pi} \tag{9}$$

and thus

$$\tau_{2^+} = \frac{1}{2}\left(\Delta C + \frac{\Delta C - \Delta C_{\mathrm{Compton}}}{\Pi} - \mathrm{PRD}\right) = 730(30)\ \mathrm{ps}, \tag{10}$$

which is in good agreement with the results obtained using the slope method (Fig. 14b). This result has been verified by an analogous Compton-background analysis on the 212-keV ground-state transition, thus with $E_{\mathrm{ref.}} = 352$ keV and EXILL triggering on the 497-keV γ ray. Although the peak-to-background ratio and the time shift between the full-energy and Compton events at 212 keV are different than the reversed case presented in Fig. 14, the results after corresponding time correction are consistent within errors. This is expected when the full-energy peak of both the feeding and decaying γ rays are sitting on Compton background [36]. Otherwise, it is important to investigate for the peak-to-background ratios of both γ rays, as after multiple gating, the Compton background can be eliminated for certain energies and thus not necessarily for both γ-ray energies each completely.

A similar Compton-background analysis for the determination of the lifetime of the first 4^+ state in ^{100}Zr is presented in Fig. 15. In this case no significant difference in the timing of the full-energy and the Compton events can be observed at 497 keV. According to the peak-to-background ratio of $\Pi = 1.8(2)$ an additional error of 10 ps is taken into account for the determination of the centroid difference corresponding to the relative timing uncertainty of the Compton events. Thus the result here is $\tau_{4^+} = 42(8)$ ps. Although the large background may have a small contribution of the 511 keV annihilation γ-rays, the result obtained is in good agreement with the literature value indicated in Fig. 15b.

4. Conclusion

Large high-efficiency Ge and $LaBr_3$(Ce) detector arrays have been assembled and installed at the intense cold-neutron guide PF1B of the ILL. The EXILL&FATIMA spectrometer allows for the first time to perform fast-timing lifetime measurements in prompt γ-ray spectroscopy experiments on exotic neutron-rich fission fragments. Extensive calibration measurements have been performed to test the precision of such a high-granularity fast-timing array by using the mirror symmetric GCD method. This new approach delivers a new fast-timing-array spectrometer constant, namely the mean prompt response difference between the start

and stop events of the FATIMA set-up. Whereas the timing between single detector pairs is sensitive to the position and the extensions of the γ-ray emitter, the 3-dimensional centrally symmetric fast-timing array in combination with the GCD method is shown to largely cancel the geometrical timing effects. In addition, possible systematic errors due to the typical timing asymmetries and time drifts are also cancelled. Over 5 weeks of operation, no significant change of the prompt response difference curve has been detected. The prompt response difference was measured for the total dynamic range of the FATIMA set-up ranging from 40 keV up to 6.8 MeV with an overall precision of 10 ps. The fast-timing performance of the presented FATIMA set-up, given as the γ–γ coincidence FWHM of prompt time spectra, is 270–500 ps for energies larger than 100 keV. This allows to access lifetimes of nuclear excited states below 300 ps with precision better than 10 ps with only 1000–2000 Ge–$LaBr_3$–LaBr3 or Ge–Ge–$LaBr_3$–$LaBr_3$ coincidences. Thanks to the high-efficiency EXILL array, around 100 neutron-rich isotopes with fission yields larger than 0.1% will be investigated from the data sets acquired using ^{235}U and ^{241}Pu targets during the EXILL&FATIMA campaign in 2013.

Extensive studies on the influence of the background in γ–γ fast-timing experiments have been performed. Inter-detector Compton scattering has been shown to be important only for adjacent $LaBr_3$-detector combinations. Such cross-talk γ–γ coincidences have been excluded from the analysis, resulting in a geometrical shielding for the other detector pairs, and thus a Compton suppression. Thanks to high-resolution gating using EXILL, the Compton background in the doubly gated (Ge+$LaBr_3$) $LaBr_3$ coincidence spectrum is remarkably reduced, even to negligible contributions in special cases. Otherwise, the proposed time-correction procedure related to the timing of the Compton background underneath the full-energy peak of interest has been shown to be accurate and reliable. For peak-to-background ratios larger than 2 and for about 2000 γ–γ events, the error of this time-correction procedure is smaller than 10 ps. In prompt fission–fragment experiments as proposed in this article, a better lifetime precision can be obtained using quadruple Ge–Ge–$LaBr_3$–$LaBr_3$ gates as thousands of γ rays produce massive Compton background that cannot be effectively reduced or even fully suppressed using only one EXILL gate. In any case, a range of gates are possible in the nucleus of interest and on some of the transitions in complementary fission fragments to increase the statistics.

Acknowledgement

This work was supported by NuPNET, by contract 05P12PKNUF of the German BMBF, by contract DNC7RP01/4 of the British STFC, by the ERA-NET NuPNET call for translational joint activities by contract PRI PIMNUP-2011-1338 of the Spanish MINECO and the projects FPA2010-17142 and CPAN (CSD 2007-00042) funded by the Spanish MINECO. The EXILL&FATIMA campaign would not have been possible without the support of several services at the ILL and the LPSC of Grenoble. We are grateful to the EXOGAM collaboration for the loan of the detectors and to GANIL for assistance during installation and dismantling of the array. We are also grateful for the provision of high-quality fast-timing equipment by the FATIMA collaboration.

References

[1] I. Ahmad, W.R. Phillips, Reports on Progress in Physics 58 (1995) 1415.
[2] E. Cheifetz, et al., Physical Review Letters 25 (1970) 38.
[3] M. Bücher, et al., Physical Review C 41 (1990) 1115.
[4] W. Urban, et al., The European Physical Journal A – Hadrons and Nuclei 16 (2003) 11.
[5] H. Mach, R.L. Gill, M. Moszyński, Nuclear Instruments and Methods in Physics Research Section A 280 (1989) 49.
[6] M. Moszyński, H. Mach, Nuclear Instruments and Methods in Physics Research Section A 277 (1989) 407.
[7] W. John, F.W. Guy, J.J. Wesolowski, Physical Review C 2 (1970) 1451.
[8] A.G. Smith, et al., Physical Review Letters 73 (1994) 2540.
[9] G. Mamane, et al., Nuclear Physics A 454 (1986) 213.
[10] A.G. Smith, et al., Journal of Physics G: Nuclear and Particle Physics 28 (2002) 2307.
[11] H. Abele, et al., Nuclear Instruments and Methods in Physics Research Section A 562 (2006) 407.
[12] W. Urban, et al., Journal of Instrumentation 8 (2013) P03014.
[13] J. Simpson, et al., Acta Physica Hungarica New Series, Heavy Ion Physics 11 (2000) 159.
[14] L.M. Fraile, et al., Nuclear Instruments and Methods in Physics Research Section A 701 (2013) 235.
[15] J.-M. Régis, et al., Nuclear Instruments and Methods in Physics Research Section A 726 (2013) 191.
[16] P. Mutti, et al., in: Proceedings of ICALEPCS 2011, Grenoble France, 2011, p. 935.
[17] N. Saed-Samii, Diploma Thesis, University of Cologne, 2013, unpublished.
[18] P. Dorenbos, J.T.M. de Haas, C.W.E. van Eijk, IEEE Transactions on Nuclear Science NS-42 (1995) 2190.
[19] G. Molnár, Z. Révay, T. Belgya, Nuclear Instruments and Methods in Physics Research Section B 213 (2004) 32.
[20] J.-M. Régis, Ph.D. Thesis, University of Cologne ⟨http://kups.ub.uni-koeln.de/4290/⟩, 2011.
[21] M.J. Martin, Nuclear Data Sheets 114 (2013) 1497.
[22] H. Mach, et al., Journal of Physics G: Nuclear Particle Physics 31 (2005) S1421.
[23] K.E.G. Löbner, in: W.D. Hamilton (Ed.), The Electromagnetic Interaction in Nuclear Spectroscopy, North-Holland, New York, 1975, p. 173.
[24] Z. Bay, Physics Review 77 (1950) 419.
[25] H. Mach, et al., Nuclear Physics A 523 (1991) 197.
[26] J.-M. Régis, et al., Nuclear Instruments and Methods in Physics Research Section A 684 (2012) 36.
[27] L.G. Hyman, Review of Scientific Instruments 36 (1965) 56.
[28] M. Moszyński, et al., Nuclear Instruments and Methods in Physics Research Section A 567 (2006) 31.
[29] M. Moszyński, et al., IEEE Transactions on Nuclear Science NS-53 (5) (2006) 2484.
[30] B. Bengtson, M. Moszyński, Nuclear Instruments and Methods 81 (1970) 109.
[31] M. Moszyński, et al., Nuclear Instruments and Methods 134 (1976) 77.
[32] E. Browne, J.K. Tuli, Nuclear Data Sheets 114 (2013) 1849.
[33] J. Glodo, et al., IEEE Transactions on Nuclear Science NS-52 (5) (2005) 1805.
[34] T.W. Burrows, et al., Nuclear Data Sheets 109 (2008) 1879.
[35] T.J. Paulus, IEEE Transactions on Nuclear Science NS-32 (3) (1985) 1242.
[36] J.-M. Régis, et al., Nuclear Instruments and Methods in Physics Research Section A 622 (2010) 83.
[37] N. Nica, J. Cameron, B. Singh, Nuclear Data Sheets 113 (2012) 1.
[38] B. Singh, Nuclear Data Sheets 109 (2008) 297.